2008

Characterization of Aerosols Containing Zn, Pb, and Cl from an Industrial Region of Mexico City

Ryan C. Moffet
University of California

Yury Desyaterik
Pacific Northwest National Laboratory

Rebecca J. Hopkins
Lawrence Berkeley National Laboratory

Alexei V. Tivanski
Lawrence Berkeley National Laboratory

Mary K. Gilles
Lawrence Berkeley National Laboratory

See next page for additional authors

Characterization of Aerosols Containing Zn, Pb, and Cl from an Industrial Region of Mexico City

RYAN C. MOFFET,[†,§] YURY DESYATERIK,[‡] REBECCA J. HOPKINS,[§] ALEXEI V. TIVANSKI,[§] MARY K. GILLES,[§] Y. WANG,[†] V. SHUTTHANANDAN,[‡] LUISA T. MOLINA,[∥,⊥] RODRIGO GONZALEZ ABRAHAM,[∥] KIRSTEN S. JOHNSON,[⊥] VIOLETA MUGICA,[#] MARIO J. MOLINA,[†] ALEXANDER LASKIN,*[,‡] AND KIMBERLY A. PRATHER*[,†]

Department of Chemistry and Biochemistry, University of California, San Diego, California 92093-0314, W.R. Wiley Environmental Molecular Sciences Laboratory, Pacific Northwest National Laboratory, Richland, Washington 99352, Chemical Sciences Division, Lawrence Berkeley National Laboratory, Berkeley, California 94720-8226, Molina Center for Energy and the Environment (MCE²), La Jolla, CA, Department of Chemistry, Massachusetts Institute of Technology, Cambridge, Massachusetts 02139-4307, and Applied Chemistry, Universidad Autónoma Metropolitana-Azcapotzalco, Av. San Pablo 180, México D.F. 02200

Received December 6, 2007. Revised manuscript received June 16, 2008. Accepted July 21, 2008.

Recent ice core measurements show lead concentrations increasing since 1970, suggesting new nonautomobile-related sources of Pb are becoming important worldwide (*1*). Developing a full understanding of the major sources of Pb and other metals is critical to controlling these emissions. During the March, 2006 MILAGRO campaign, single particle measurements in Mexico City revealed the frequent appearance of particles internally mixed with Zn, Pb, Cl, and P. Pb concentrations were as high as 1.14 μg/m^3 in PM_{10} and 0.76 μg/m^3 in $PM_{2.5}$. Real time measurements were used to select time periods of interest to perform offline analysis to obtain detailed aerosol speciation. Many Zn-rich particles had needle-like structures and were found to be composed of ZnO and/or $Zn(NO_3)_2 \cdot 6H_2O$. The internally mixed Pb−Zn−Cl particles represented as much as 73% of the fine mode particles (by number) in the morning hours between 2−5 am. The Pb−Zn−Cl particles were primarily in the submicrometer size range and typically mixed with elemental carbon suggesting a combustion source. The unique single particle chemical associations measured in this study closely match signatures indicative of waste incineration. Our findings also show these industrial emissions play an important role in heterogeneous processing of NO_y species. Primary emissions of metal and sodium chloride particles emitted by the same source underwent heterogeneous transformations into nitrate particles as soon as photochemical production of nitric acid began each day at ~7 am.

Introduction

Particulate air pollution is correlated with increased morbidity and mortality through cardiovascular and pulmonary effects (*2*). Although relatively little is known about the specific chemical constituents responsible for the adverse health effects, metal-containing particles are implicated in a number of studies (*3–5*). The solubility of metal ions present in particles affects their mobility in the human body while their oxidation state greatly affects their toxicity (*5*). Other factors such as particle size and shape determine how deep into the respiratory tract a particle may travel. Smaller particles with a compact morphology penetrate deeper into the lungs where they are more likely to be retained by the body (*6–8*). Anthropogenic particles created by high temperature processes (e.g., combustion and ore processing) possess many of the properties responsible for adverse health effects.

In urban areas, anthropogenic sources of submicron metal-containing particles are plentiful. For example, the burning of fossil fuel leads to the association of Ni and V within particles (*9*). Prior to 2000, tetra-ethyl-lead was used as a gasoline additive in many countries and resulted in traffic related emissions of submicron lead particles (*10*). In industrial areas, smelting produce particulate emissions rich in heavy metals (*11*). Combustion of municipal waste produces submicron particles composed of Zn, Pb, and Cl as well as numerous other metals (*12*). Zn and Pb are often found to be internally mixed in particles detected in different geographic locations (*10*). Dust particles are predominantly supermicrometer sizes and when stirred up through anthropogenic activities (such as construction and/or vehicular traffic), they effectively transport metals into the atmosphere (*13*). Each of these metal sources emits particles with unique compositions which can ideally be identified using the appropriate combination of analytical techniques.

To characterize metal-containing particles in the Mexico City metropolitan area (MCMA), an extensive suite of aerosol measurement and sampling techniques was used. In the past decade, several field studies in MCMA have employed a variety of instrumentation to address particulate pollution and air quality issues (*14–17*). Researchers found the northern part of the city is characterized by high concentrations of industrial emissions, in particular, Zn- and Pb-containing particles (*14, 17, 18*). Notably, blood Pb levels in children in the northeastern part of the city were 10.9% higher than children in the southwestern region (*19*). The elevated metal concentrations in the northern MCMA have been generally attributed to industry, and the exact identity has not been determined.

The research presented herein was carried out during the Megacity Initiative: Local and Global Research Observations (MILAGRO) field study held in March 2006 (see http://mce2.org/). As part of the MILAGRO study, a sampling site (T0) was established in northern MCMA and was impacted by industrial, vehicle, and residential emission sources (*20*). Single particle mass spectrometry was used to identify a unique period with a high abundance of Zn and Pb particles on March 24, 2005. Detailed studies using complementary techniques provide information on particle chemistry, metal speciation, size, mixing state, and morphology of metal-

* Address correspondence to either author. Phone: 858-822-5312 (K.A.P.); 509-371-6129 (A.L.). E-mail: kprather@ucsd.edu (K.A.P.); Alexander.Laskin@pnl.gov (A.L.).
† University of California.
‡ Pacific Northwest National Laboratory.
§ Lawrence Berkeley National Laboratory.
∥ Molina Center for Energy and the Environment.
⊥ Massachusetts Institute of Technology.
Universidad Autónoma Metropolitana-Azcapotzalco.

10.1021/es7030483 CCC: $40.75
Published on Web 08/29/2008

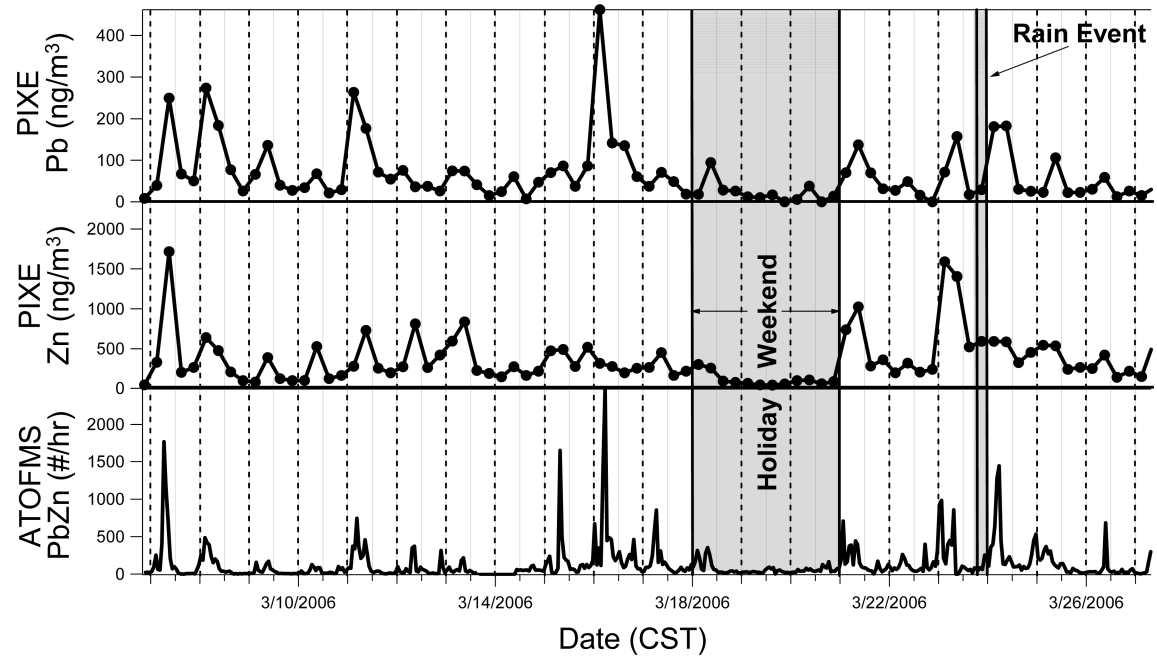

FIGURE 1. Time series of unscaled ATOFMS counts of Zn- and/or Pb-containing particles compared with the PIXE bulk mass concentrations of Zn and Pb. The major and minor tick marks occur at 12 am and 12 pm, respectively. PIXE data are shown for 0.36−2.5 μm particles.

containing particles along with quantitative mass loadings. Spatial, temporal, physical, and chemical information on these particles suggests they were produced by local waste incineration. Single particle mass spectrometry and electron microscopy provide unique information that is used to show not only the concentration and source of these industrial emissions, but also insight into the atmospheric processing these particles undergo after they are emitted. Microscopy and spectro-microscopic techniques provide morphology and oxidation state information that is crucial for elucidating the potential environmental effects of these particles.

Experimental Section

Sampling site T0 was located in the northern part of MCMA at the "Instituto Mexicano del Petroleo" (IMP) at 19°29′23.60 N, 99°08′55.60W and 2200 m above sea level. The site was surrounded by industrial and residential areas as well as roads with intensive traffic (*16*). A number of complementary techniques were used in this study. The aerosol time-of-flight mass spectrometer (ATOFMS) measures real-time single particle size and composition with hourly time resolution. Computer controlled scanning electron microscopy with energy dispersive X-ray analysis (CCSEM/EDX) provides quantitative information on thousands of the substrate collected particles. Scanning transmission X-ray microscopy with near edge X-ray spectroscopy (STXM/NEXAFS) provides off-line molecular speciation of individual particles. Proton induced X-ray emission (PIXE) yields time-resolved bulk mass concentrations of $Z > 23$ elements with a 6 h time resolution. A more detailed description of these techniques is presented in the Supporting Information.

Results and Discussion

Historically, the high concentrations of Zn and Pb particles in the northern MCMA have broadly been attributed to industrial processes (*14, 16, 17*). The time series derived from the ATOFMS and PIXE data presented in Figure 1 show episodes of particles containing Pb and Zn were common throughout the study. Table 1 shows the average, maximum, and minimum concentrations for Zn and Pb in the PM_{10} and $PM_{2.5}$ size ranges determined with high volume filters. The highest PM_{10} levels for Zn and Pb were 1.4 and 1.14 $\mu g/m^3$, respectively, with the majority of the Pb mass in $PM_{2.5}$. The episodes of Pb and Zn particles usually occurred between the night and mid morning (12−10 am CST). Calculated back trajectories indicate that during these periods the air masses originated from the industrial region of the city, north of the sampling site (*20*). Previous studies have attributed the source of the high Zn and/or Pb concentration to industrial emissions (*14, 17, 18*). The source assignment of industrial emissions is supported by the low concentrations of these particles during the holiday weekend of March 18−20 as highlighted in Figure 1.

TABLE 1. Twenty-four Hour Average PM_{10} and $PM_{2.5}$ ($\mu g/m^3$) for Pb and Zn Determined between March 6 and 30

	Pb PM_{10}	Pb $PM_{2.5}$	Zn PM_{10}	Zn $PM_{2.5}$
average	0.22	0.15	0.50	0.34
min	0.06	0.01	0.14	0.04
max	1.14	0.76	1.4	0.49

On March 24, 5:15−5:30 CST the ATOFMS measured a peak in the percentage of particles containing Zn and Pb as indicated in Figure 1. This paper focuses on this episode, serving as a representative event that occurred nearly every day of the study. This particular event followed a heavy rainfall that significantly decreased the background aerosol concentrations, thus increasing the ability to study the industrial plumes microscopically.

Particle Classification. A rule based classification scheme showed that following the heavy rain event, the number percentage of particles containing Pb or Zn was 61% (by ATOFMS) to 73% (by CCSEM/EDX). The classification scheme shown in Figure 2 and detailed in the Supporting Information, was motivated by the observation that the majority of particles contained Pb, Zn, Fe, and/or Na. Particles were first separated into those containing metals (Me > 0) or no metals (Me = 0). The metal-containing particles were further separated into two classes; those containing Zn and/or Pb (Me > 0, ZnPb > 0), and those without Zn or Pb (Me > 0, Pb = 0, Zn

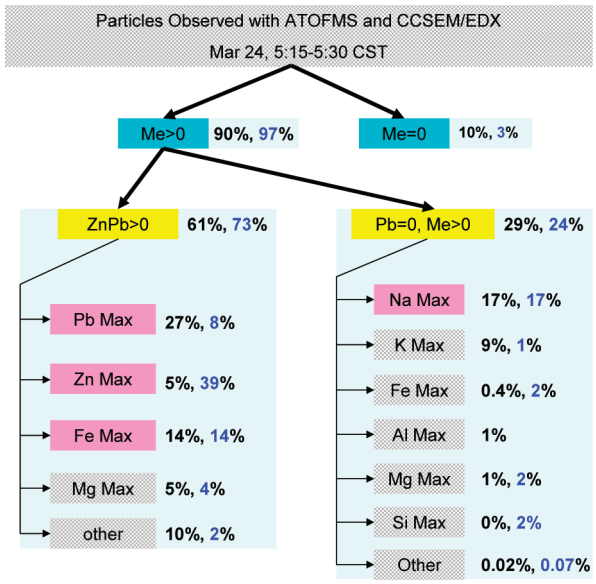

FIGURE 2. Rule based classification from ATOFMS and CCSEM/EDX data. Percent of particles in a class out of the total number of analyzed particles is indicated in black (ATOFMS) and blue (CCSEM/EDX). Pb or Zn in particles is indicated by ZnPb > 0. The size range analyzed for both instruments was approximately 0.2−2 μm.

= 0). The label "max" indicates that those particular metals made up the maximum signal out of all of the elements analyzed.

The percentages shown in black and blue in Figure 2 represent the relative number of particles classified for the CCSEM/EDX and the ATOFMS data sets, respectively. Figure 2 shows that, a majority of the particles, 61−72% by number, contained Pb or Zn, leaving a PbZn = 0 class mixed with other metals including Na, Pb, Zn, K, Cu, Cr, and Cd; 3 and 12% of the Me > 0 particles contained the health relevant metals Cd and Cr. The two data sets were in excellent agreement for the Na-max, Fe-max, and Mg-max particle classes. In general, the CCSEM/EDX and ATOFMS results agreed except for the higher percentages of the K max and Pb max classes given by the ATOFMS, reflecting the enhanced sensitivity of the ATOFMS toward these metals. In fact, 80% of the Pb max particles were internally mixed with Zn, so it is likely that many Zn-rich particles detected by the CCSEM are actually contained in the ATOFMS Pb max class.

Particle Mixing State and Source Profiles. The chemical mixing state of a particle describes which chemical species are contained in the same particle. Mixing state information from ATOFMS and CCSEM are presented in the Supporting Information while the most salient findings are reported here. ATOFMS and CCSEM/EDX showed that ZnPb > 0 particles are internally mixed with Cl, Na, K, P, S, and a multitude of other elements. This mixing state can be directly compared to source mixing states measured in previous source characterization studies. Tan et al. (2002) compared single particle mass spectra of particles collected from nonferrous smelters and municipal waste incinerators and showed that these two sources had many common elemental markers with the exception of P and Cl which were more abundant in incineration (*21*). Figure 3 compares the Me > 0 particles reported here with the source samples from municipal waste incineration and copper smelting from Tan et al. (*21*). The Me > 0 and nonferrous smelter particles did have sulfur at $m/z = -32$ and -64 in common, a marker not reported for incineration by Tan et al. However, the dot product of the percent contribution vectors shown in Figure 3 is 0.88 between incineration and Me > 0, while it is 0.53 between Me > 0 and nonferrous smelting. The best match with the

FIGURE 3. Comparison of MCMA aerosol on Mar 24 from 5:15−5:30 am with two industrial sources. The color is proportional to the percentage of particles in the sample given on the vertical axis containing a particular marker indicated by the horizontal axis; this percentage is also indicated inside of each box. Mexico City metal aerosol more closely matches waste incineration than smelting. Key elemental tracers include Pb, Zn, Cl, and P. The ATOFMS data used for this figure is the "Me > 0" particle set defined in Supporting Information Table S1. (* Source data obtained from Tan, 2002 (*21*).)

Me > 0 particles from Mexico City is with incineration, with the key elemental tracers P and Cl both abundantly present in each sample.

The mixing state analysis is further supported by PIXE measurements from which we have applied a factor analysis to extract an industrial factor showing strong contributions from Pb, Zn, Cr, and Cl. As shown in Supporting Information Table S2, the strongest associations within the industrial factor were, from weakest to strongest, between Cl, Na, Zn, Pb, Cr, and P. This was similar to the mixing state identified by the ATOFMS and CCSEM/EDX. Furthermore, many of these elements were key markers distinguishing incineration from smelting in the work of Tan et al. (*21*). However, the PIXE factor analysis was unable to identify associations with nitrogen and carbon. Thus, as described below, other complementary methods are used to obtain a more complete picture.

In addition to source identification, the mixing state may also be used to obtain more detailed chemical composition. ATOFMS shows that the Zn and Pb particles were found to be mixed with carbonaceous species such as elemental carbon (EC), aromatics, other metals, and organic species such as the oxalate ion. The ATOFMS spectra showed that at least 40% of the Pb and Zn particles were mixed with soot/EC supporting the assertion that they were generated from combustion. In Supporting Information Figure S2, it is shown that the nonmetal (Me = 0) class present in this industrial plume had a distinct aromatic hydrocarbon signature with 75% of these particles containing aromatic markers and 8% of these particles containing Cl. Furthermore, 13−15% of the Pb- and Zn-containing particles were found to be internally mixed with aromatic hydrocarbons in addition to chloride. The variability and extent of particle mixing with other species (including Mn and Cu) is further quantified in the Supporting Information (Figures S1−S4).

Particle Morphology. Morphology is an important microphysical trait that relates to particle aerodynamic behavior, possible health effects (*2*), speciation (*3*), phase, formation mechanism, and source identification. The SEM images shown in Figure 4 illustrate the morphology of metal rich particles typical for this study. Nonspherical, needle-like Zn- and Pb-containing particles (panels A, B, and C), as well as spherical Zn particles containing PbFe and Mn (not shown) were detected. Figure 4a shows Zn-containing particles internally mixed with soot, which is consistent with ATOFMS results indicating that at least 40% of the Zn-containing particles were mixed with elemental carbon. SEM/EDX analysis confirmed that the needle like structures shown in Figure 4c were mostly composed of Zn and O with only minor amounts of other elements suggesting a similarity to previously reported tetrahedral ZnO particles (*22*). ATOFMS optical measurements also indicated that the particles containing Zn and Pb were nonspherical with effective densities that exceeded 2.4 g/cm^3 (*23*). A high abundance of cubic

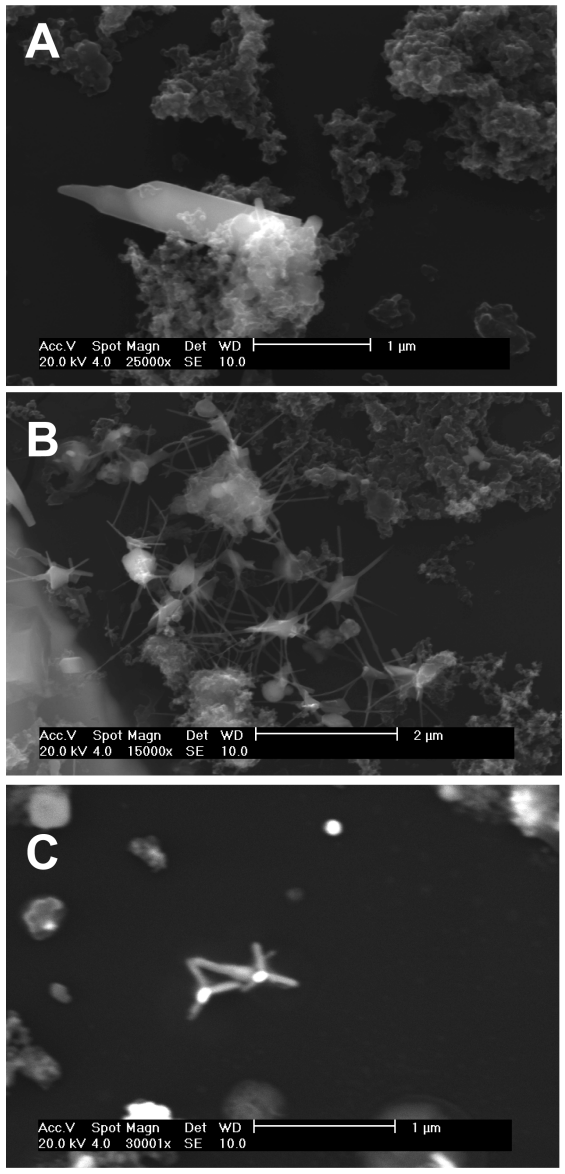

FIGURE 4. Images illustrating the morphology of metal containing particles observed in Northern Mexico City. (A) Zn containing crystal attached to soot; (B) Needle-like particles containing Pb, Zn, and Cl; (C) Tetrahedral Zn containing particles with compact Pb rich particles.

NaCl particles were also observed to be internally and externally mixed in the same samples as the metal rich particles, indicating they were likely produced by the same source.

Speciation and Phase of Zn- and Pb-Contaning Particles. Using STXM/NEXAFS, two major particle classes were distinguished from one another based on morphology and NEXAFS spectra. Representative STXM images are shown in Figure 5. Particles shown in Figure 5a (type A) were found to be internal mixtures of Zn, EC, and K, whereas particles in Figure 5b (type B) were found to be needle-like Zn particles discussed previously (*22*). The presence of EC and K in type A was confirmed with the corresponding carbon K-edge NEXAFS spectra.

To elucidate the chemical speciation of Zn-containing particles, the Zn L-edge NEXAFS spectra of ZnO, ZnS, $Zn(NO_3)_2 \cdot 6H_2O$, $ZnCl_2$, $ZnSO_4$ standard reference materials were measured for comparison with particles of types A and B. Representative normalized Zn L-edge NEXAFS spectra for both particle classes and $Zn(NO_3)_2 \cdot 6H_2O$ and ZnO standards are shown in Figure 5. The spectra in Figure 5a and b correspond to the average spectrum collected over six single particles located in different regions of the substrate. ZnS, $ZnSO_4$, and $ZnCl_2$ standards did not match the spectra of the Zn-containing particles. The similarities in the spectra of the $Zn(NO_3)_2 \cdot 6H_2O$ and ZnO particles with those of particle types A and B, provide chemical identification of these two types. While the spectrum of particle type B matches well with that of ZnO, small deviations between the spectra of particle type A and $Zn(NO_3)_2 \cdot 6H_2O$ are observed at ~1025 eV and ~1050 eV. These deviations may arise due to the presence of minor amounts of other Zn compounds and/or unidentified components in the ambient particles.

Heterogeneous Chloride-to-Nitrate Chemistry. Different emission sources are expected to be associated with specific particle chemistry and morphology. Waste incineration, has been shown to emit Pb, Zn, and Na chloride particles (*12, 24, 25*). Nearly 100% of the Pb and Zn particles contained Cl (Supporting Information Figure S2). Furthermore, $ZnCl_x$ and $NaCl_x$ clusters were common in the ATOFMS spectra. Particles containing chloride can undergo atmospheric processing where the chloride is displaced by nitrate:

$$MCl_{n(s)} + nHNO_{3(g)} \rightarrow M(NO_3)_{n(s)} + nHCl_{(g)} \qquad (R1)$$

where M represents Zn, Pb, Na, or K. The CCSEM/EDX and ATOFMS show the Zn and Pb particles were internally mixed with Cl and NO_3. As shown in Figure 6, the ATOFMS measured a strong temporal anticorrelation between nitrate and chloride for Pb-, Zn-, and Na-containing particles. Each morning, the initial spike of chloride containing particles was followed by the appearance of the same particles enriched in nitrate and depleted in chloride. The reaction started at approximately 7 am each morning and peaked at ~12−2 pm each day. The $ZnCl_2$ and NaCl particles began to be transformed to $Zn(NO_3)_2$ and $NaNO_3$ particles as soon as the HNO_3 began to form in the mornings (*27*). Thus, the displacement reaction shown in R1 explains the $Zn(NO_3)_2$ particles observed with the STXM/NEXAFS.

The extent of chemical processing may be different because particles contain different amounts of reactive chloride. CCSEM/EDX and ATOFMS show that Cl is present in over 70% of Zn- and Pb-containing particles (Supporting Information Figure S2) whereas "Pb max" particles contain larger amount of Cl compared to the "Zn max" particles (Supporting Information Figure S4). Also, all of the PbZn > 0 particles contained Na, therefore the chloride was also associated with Na within these same particles. Because these industrial particles represented as much as 73% of the total particles during morning hours, their presence can strongly influence the chemistry of aerosols in the MCMA as demonstrated in Figure 6.

Sources of Metal-Containing Particles in Mexico City. Numerous industrial emission sources exist in northern Mexico City. The emissions inventory for the immediate area (within 5 km) obtained by the Secretary of the Environment of the Government of the Federal District (SMA/GDF) indicates that metallurgical sources release a substantial fraction of the $PM_{2.5}$ compared to other industries. While smelting could be a source of some of the particles observed here, previous studies do not report large amounts of Cl associated with smelter emissions. However, Dall'Osto et al. have reported such associations with chloride in a recent study of steelworking (*26*). Earlier metallurgical source studies also noted high SO_2 concentrations within smelter plumes. Such plumes of SO_2 were not reported for MCMA where only weak correlations were observed among SO_2, Zn, and Pb. Zn- and Pb-containing particles identified by ATOFMS in this study also came from the northeast (*20*), and were not correlated with SO_2 gas phase concentrations. One caveat to this is that a high percentage of the Me > 0 particles observed

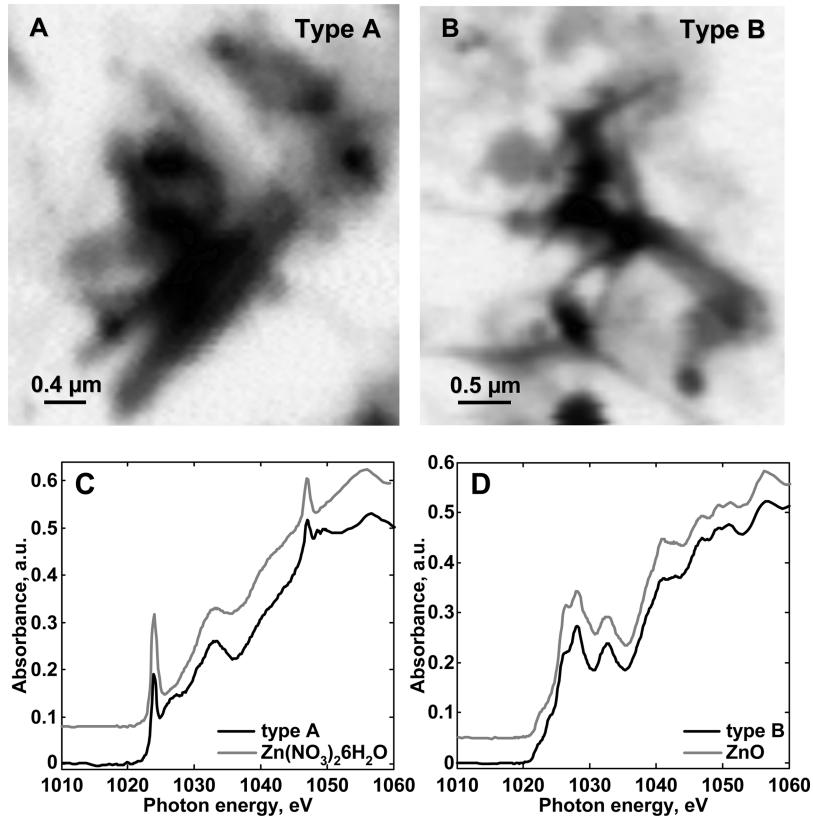

FIGURE 5. Upper panel: single energy (1024 eV) STXM images of two types of Zn containing particles observed in Northern Mexico City. (A) Zn-containing crystals internally mixed with elemental carbon; (B) - Needle-like Zn-containing particles. Lower panel: representative Zn L-edge normalized NEXAFS spectra for (C) particle type A and $Zn(NO_3)_2 6H_2O$ standard and (D) particle type B and ZnO standard.

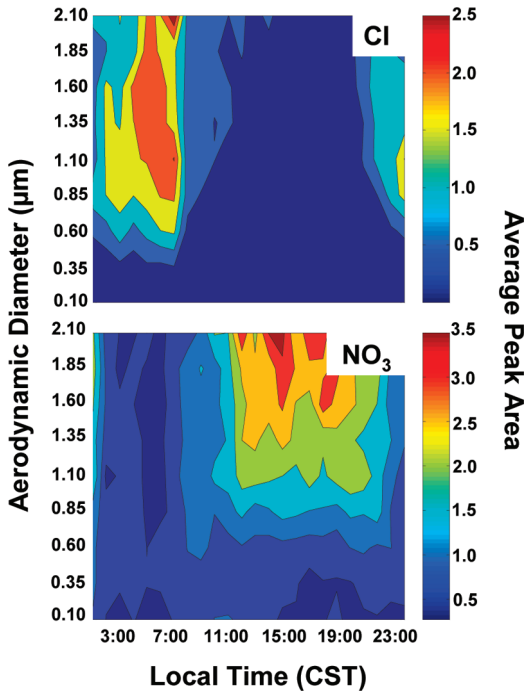

FIGURE 6. Average peak area for Cl and NO_3 as a function of time and size for Pb- and Zn-containing particles mixed with Cl. This demonstrates the displacement of chloride by nitrate within individual Pb and Zn particles.

in our study did contain primary sulfur markers at m/z −32 (S^-)and −64 (S_2^-) (Figure 3). Nevertheless, since the time trends and indicated source direction of the Cl particles reported by Salcedo et al. (*27*) and Johnson et al. (*18*) are similar to those observed for the Zn/Pb/Cl-containing particles studied here, it is highly likely that the chloride particles observed in these previous studies came from the same source.

Municipal and hazardous waste incineration have been shown to emit Pb, Zn, and Cl particles (*21, 28–31*). For this source, the Cl is primarily from the burning of plastics such as polyvinyl chloride and paper, whereas the Pb and Zn can be produced from a variety of waste materials. Electronic waste represents a good example of a waste stream that contains an abundance of these three elements. The PIXE, ATOFMS, and CCSEM/EDX analyses presented here indicate these elements are internally mixed, while associations with carbonaceous material suggest these particles result from combustion. ATOFMS identified organic particles that contained an abundance of aromatic markers that may indicate the presence of diphenyl or other similar aromatic compounds typical for incineration emissions. Incineration is not currently listed in the emissions inventory for the MCMA; however, multiple waste incinerators exist in the northern part of Mexico City (*20*).

A combination of techniques was used to probe the mixing state, morphology, oxidation state and heterogeneous chemistry of Zn- and Pb-containing particles. A time series analysis indicates metal-rich particles peaked at the sampling site during the early morning hours. This is consistent with previous studies showing high Zn and Pb concentrations correlated with early morning air masses from the northeastern MCMA. Evidence of industrial incineration was supported by the time series data showing the lowest metal particle concentrations during a holiday weekend. Direct comparison of our data with single particle source samples from waste incineration supports incineration as the most probable source of these particles. Moreover, three different

techniques confirmed that many of the ZnCl-rich particles were mixed with EC, which additionally supports combustion as the source of these particles.

Complementary ATOFMS, CCSEM/EDX, and PIXE data show that particles containing Zn and/or Pb are mixed with Cl and nitrate. ATOFMS measured the conversion to metal nitrate particles immediately following the metal-chloride particle spikes. The time lag of nitrate behind chloride suggests a heterogeneous displacement reaction of metal chlorides with nitric acid. This assertion is supported by STXM/NEXAFS results showing Zn rich particles composed of $Zn(NO_3)_2 \cdot 6H_2O$. Because these particles sometimes dominated number concentrations in the 0.2−1 μm range, this heterogeneous chemistry may be an important source of submicron nitrate mass while impacting the gas phase NO_y budget.

The frequent observation of these metal-rich particles in an urban area with a high population density also has important implications for health effects. The largest fraction of the Pb-containing particles is less than 2.5 μm, meaning that these particles may be efficiently inhaled. Also, there may be important health ramifications if salts such as $Pb(NO_3)_2$ are formed because lead nitrate is soluble, and therefore more mobile within the human body.

Acknowledgments

We thank the individuals who helped out at the T0 site. The UCSD, the MIT, and the MCE^2 groups acknowledge support provided by the U.S. National Science Foundation (ATM-0528227), the Atmospheric Science Program of the office of Biological and Environmental Research (ASP/OBER) of the U.S. Department of Energy (DOE), (grant DE-FG02-05ER63980). The PNNL and the LBNL research groups acknowledge support provided by ASP/OBER DOE. The AUMA research group acknowledges support provided by Mexican Comision Ambiental Metropolitana, The CCSEM/EDX and PIXE particle analyses were performed in the Environmental Molecular Sciences Laboratory, a national scientific user facility sponsored by the Department of Energy's Office of Biological and Environmental Research at Pacific Northwest National Laboratory. PNNL is operated by the U.S. Department of Energy by Battelle Memorial Institute under contract DE-AC06-76RL0. STXM/NEXAFS experiments at the ALS were partially supported by the Director, Office of Science, Office of Basic Energy Sciences, Division of Chemical Sciences, Geosciences, and Biosciences of the U.S. Department of Energy at Lawrence Berkeley National Laboratory under Contract No. DE-AC02-05CH11231.

Supporting Information Available

Details regarding experimental procedures, rules based particle classification, and single particle mixing state. This material is available free of charge via the Internet at http://pubs.acs.org.

Literature Cited

(1) Osterberg, E.; Mayewski, P.; Kreutz, K.; Fisher, D.; Handley, M.; Sneed, S.; Zdanowicz, C.; Zheng, J.; Demuth, M.; Waskiewicz, M.; Bourgeois, J. Ice core record of rising lead pollution in the north pacific atmosphere. *J. Geophys. Lett.* **2008**, 35.

(2) Pope, C. A.; Dockery, D. W. Health effects of fine particulate air pollution: Lines that connect. *J. Air Waste Manage.* **2006**, *56*, 709–742.

(3) Dreher, K. L.; Jaskot, R. H.; Lehmann, J. R.; Richards, J. H.; McGee, J. K.; Ghio, A. J.; Costa, D. L. Soluble transition metals mediate residual oil fly ash induced acute lung injury. *J. Toxicol. Environ. Health* **1997**, *50*, 285–305.

(4) Florea, A. M.; Busselberg, D. Occurrence, use and potential toxic effects of metals and metal compounds. *Biometals* **2006**, *19*, 419–427.

(5) Hodgson, M. J.; Bracker, A.; Yang, C.; Storey, E.; Jarvis, B. J.; Milton, D.; Lummus, Z.; Bernstein, D.; Cole, S. Hypersensitivity pneumonitis in a metal-working environment. *Am. J. Ind. Med.* **2001**, *39*, 616–628.

(6) Schwartz, J.; Dockery, D. W.; Neas, L. M. Is daily mortality associated specifically with fine particles. *J. Air Waste Manage.* **1996**, *46*, 927–939.

(7) Londahl, J.; Massling, A.; Pagels, J.; Swietlicki, E.; Vaclavik, E.; Loft, S. Size-resolved respiratory-tract deposition of fine and Ultrafine hydrophobic and hygroscopic aerosol particles during rest and exercise. *Inhalation Toxicol.* **2007**, *19*, 109–116.

(8) Broday, D. M.; Georgopoulos, P. G. Growth and deposition of hygroscopic particulate matter in the human lungs. *Aerosol Sci. Technol.* **2001**, *34*, 144–159.

(9) Suarez, A. E.; Ondov, J. M. Ambient aerosol concentrations of elements resolved by size and by source: Contributions of some cytokine-active metals from coal- and oil-fired power plants. *Energ Fuel* **2002**, *16*, 562–568.

(10) Murphy, D. M.; Hudson, P. K.; Cziczo, D. J.; Gallavardin, S.; Froyd, K. D.; Johnston, M. V.; Middlebrook, A. M.; Reinard, M. S.; Thomson, D. S.; Thornberry, T.; Wexler, A. S. Distribution of lead in single atmospheric particles. *Atmos. Chem. Phys.* **2007**, *7*, 3195–3210.

(11) Pina, A. A.; Villasenor, G. T.; Jacinto, P. S.; Fernandez, M. M. Scanning and transmission electron microscope of suspended lead-rich particles in the air of San Luis Potosi, Mexico. *Atmos. Environ.* **2002**, *36*, 5235–5243.

(12) Linak, W. P.; Wendt, J. O. L. Toxic metal emissions from incineration - mechanisms and control. *Prog. Energy Combust. Sci.* **1993**, *19*, 145–185.

(13) Vega, E.; Mugica, V.; Reyes, E.; Sanchez, G.; Chow, J. C.; Watson, J. G. Chemical composition of fugitive dust emitters in Mexico City. *Atmos. Environ.* **2001**, *35*, 4033–4039.

(14) Flores, J.; Aldape, F.; Diaz, R. V.; Hernandez-Mendez, B.; Garcia, R. PIXE analysis of airborne particulate matter from Xalostoc, Mexico: winter to summer comparison. *Nucl. Instrum. Methods B* **1999**, *150*, 445–449.

(15) Molina, L. T.; Kolb, C. E.; de Foy, B.; Lamb, B. K.; Brune, W. H.; Jimenez, J. L.; Molina, M. J. Air quality in North America's most populous city - overview of MCMA-2003 Campaign. *Atmos. Chem. Phys.* **2007**, *7*, 2447–2473.

(16) Molina, M. J.; Molina, L. T. *Air Quality in the Mexico Megacity: An Integrated Assessment*; Kluwer Academic: Norwell, MA2002.

(17) Mugica, V.; Maubert, M.; Torres, M.; Munoz, J.; Rico, E. Temporal and spatial variations of metal content in TSP and PM10 in Mexico City during 1996−1998, *J. Aerosol Sci.* 2002, *33*, 91−102.

(18) Johnson, K. S.; de Foy, B.; Zuberi, B.; Molina, L. T.; Molina, M. J.; Xie, Y.; Laskin, A.; Shutthanandan, V. Aerosol composition and source apportionment in the Mexico City Metropolitan Area with PIXE/PESA/STIM and multivariate analysis. *Atmos. Chem. Phys.* **2006**, *6*, 4591–4600.

(19) Schnaas, L.; Rothenberg, S. J.; Flores, M. F.; Martinez, S.; Hernandez, C.; Osorio, E.; Perroni, E. Blood Lead Secular Trend in a Cohort of Children in Mexico City (1987−2002). *Environ. Health Perspect.* **2004**, *112*, 1110–1115.

(20) Moffet, R. C.; de Foy, B.; Molina, L. T.; Molina, M. J.; Prather, K. A. Measurement of ambient aerosols in northern Mexico City by single particle mass spectrometry. *Atmos. Chem. Phys.* **2008**, *8*, 4499–4516.

(21) Tan, P. V.; Fila, M. S.; Evans, G. J.; Jervis, R. E. Aerosol laser ablation mass spectrometry of suspended powders from PM sources and its implications to receptor modeling. *J. Air Waste Manage.* **2002**, *52*, 27–40.

(22) Bradley, J. P.; Goodman, P.; Chan, I. Y. T.; Buseck, P. R. Structure and evolution of fugitive particles from a copper smelter. *Environ. Sci. Technol.* **1981**, *15*, 1208–1212.

(23) Moffet, R. C.; Qin, X.; Rebotier, T.; Furutani, H.; Prather, K. A. Chemically Segregated Optical and Microphysical Properties of Ambient Aerosols Measured in a Single Particle Mass Spectrometer *J. Geophys. Res., [Atmos.]* **2008**, in press, doi: 10.1029/2007JD009393.

(24) Wu, C. Y.; Biswas, P. An equilibrium-analysis to determine the speciation of metals in an incinerator. *Combust. Flame* **1993**, *93*, 31–40.

(25) Eighmy, T. T.; Eusden, J. D.; Krzanowski, J. E.; Domingo, D. S.; Stampfli, D.; Martin, J. R.; Erickson, P. M. Comprehensive approach toward understanding element speciation and leaching behavior in municipal solid-waste incineration electrostatic precipitator ash. *Environ. Sci. Technol.* **1995**, *29*, 629–646.

(26) Dall'Osto, M.; Booth, M. J.; Smith, W.; Fisher, R.; Harrison, R. M. A study of the size distributions and the chemical characterisation of airborne particles in the vicinity of a large integrated steelworks. Aerosol Sci. Technol. **2008**, in press.
(27) Salcedo, D.; Onasch, T. B.; Dzepina, K.; Canagaratna, M. R.; Zhang, Q.; Huffman, J. A.; DeCarlo, P. F.; Jayne, J. T.; Mortimer, P.; Worsnop, D. R.; Kolb, C. E.; Johnson, K. S.; Zuberi, B.; Marr, L. C.; Volkamer, R.; Molina, L. T.; Molina, M. J.; Cardenas, B.; Bernabé, R. M.; Márquez, C.; Gaffney, J. S.; Marley, N. A.; Laskin, A.; Shutthanandan, V.; Xie, Y.; Brune, W.; Lesher, R.; Shirley, T.; Jimenez, J. L. Characterization of ambient aerosols in Mexico City during the MCMA-2003 campaign with aerosol mass spectrometry: results from the CENICA supersite. *Atmos. Chem. Phys.* **2006**, *6*, 925–946.
(28) Walsh, D. C.; Chillrud, S. N.; Simpson, H. J.; Bopp, R. F. Refuse incinerator particulate emissions and combustion residues for New York City during the 20th century. *Environ. Sci. Technol.* **2001**, *35*, 2441–2447.
(29) Ondov, J. M.; Wexler, A. S. Where do particulate toxins reside? An improved paradigm for the structure and dynamics of the urban mid-Atlantic aerosol. *Environ. Sci. Technol.* **1998**, *32*, 2547–2555.
(30) Hu, C. W.; Chao, M. R.; Wu, K. Y.; Chang-Chien, G. P.; Lee, W. J.; Chang, L. W.; Lee, W. S. Characterization of multiple airborne particulate metals in the surroundings of a municipal waste incinerator in Taiwan. *Atmos. Environ.* **2003**, *37*, 2845–2852.
(31) Chang, M. B.; Huang, C. K.; Wu, H. T.; Lin, J. J.; Chang, S. H. Characteristics of heavy metals on particles with different sizes from municipal solid waste incineration. *J. Hazard. Mater.* **2000**, *79*, 229–239.

ES7030483

Supporting Information to:

Characterization of Aerosols Containing Zn, Pb, and Cl from an Industrial Region of Mexico City

R.C. Moffet[1], Y. Desyaterik[2], R.J. Hopkins[3], A.V. Tivanski[3], M.K. Gilles[3], Y. Wang[1], V. Shutthanandan[2], L.T. Molina[4,5], R. Gonzalez Abraham[4], K.S. Johnson[5], V. Mugica[6], M.J. Molina[1], A. Laskin[2,*] and K.A. Prather[1*]

[1]*Department of Chemistry and Biochemistry, University of California, San Diego, CA 92093-0314*

[2]*W.R. Willey Environmental Molecular Sciences Laboratory, Pacific Northwest National Laboratory, Richland, WA 99352*

[3]*Chemical Sciences Division, Lawrence Berkeley National Laboratory, Berkeley, CA 94720-8226*

[4]*Molina Center for Energy and the Environment (MCE2), LaJolla, CA 92037*

[5]*Department of Chemistry, Massachusetts Institute of Technology, Cambridge, MA 02139-4307*

[6] *Applied Chemistry, Universidad Autónoma Metropolitana-Azcapotzalco (UAM-A). Av. San Pablo 180, México D.F.*

This supporting information contains: 6 pages of text, 2 Tables and 5 Figures

1. Experimental

A Davis Rotating drum Universal size-cut Monitoring (DRUM) impactor (*1*) and Time Resolved Aerosol Collector (TRAC) (*2,3*) were used to collect particulate matter samples for laboratory analysis. The DRUM impactor collected bulk particle samples for PIXE analysis in size ranges of 1.15–2.5μm (Stage A), 0.34–1.15μm (Stage B), and 0.07–0.34μm (Stage C) onto three Teflon strips at a fixed air flow of 10 slpm with a rotation rate of 2mm per 12 h. The TRAC sampled particles onto a rotating impaction plate containing pre-arranged microscopy substrates. In this study, each substrate was exposed for 15 minutes of sample collection while the collection plate was continually advanced to prevent particle overlap and provide time resolution. The effective aerodynamic cut-off size D_{50} of the TRAC is ~0.36 μm. Two different types of substrates were used in this study: (a) Copper 400 mesh TEM grids coated with Carbon Type-B films (Ted Pella, Inc.) for the computer controlled scanning electron microscopy with energy dispersed analysis of X-rays (CCSEM/EDX), and (b) 100-nm thick silicon nitride (Si_3N_4) membranes (Silson Ltd, Inc.) for the Scanning Transmission X-ray Microscopy with Near Edge X-ray Absorption Fine Structure spectroscopy (STXM/NEXAFS).

Aerosol Time-of-Flight Mass Spectrometry (ATOFMS). The ATOFMS was a single particle mass spectrometer used for the MILAGRO study and is described elsewhere (*4*). The ATOFMS analyzes sizes between 200 – 3000 nm. The single particle mass spectra, size, scattering intensity, and temporal information were imported into the MATLAB YAADA database (*http://www.yaada.org/*) (*5*).

Proton Induced X-Ray Emission (PIXE). PIXE analysis was done shortly after the MILAGRO campaign at the Environmental Molecular Sciences Laboratory (EMSL)

at Pacific Northwest National Laboratory (PNNL). Experimental procedures have been described in detail elsewhere (*6*). Briefly, Teflon substrates mounted on a special sample holder were placed inside a vacuum chamber evacuated to 2×10^{-7} Torr. A 3.5 MeV proton beam was used for PIXE analysis and the spectra were evaluated by the GUPIX program (*7*). Concentrations of elements were determined by calibration to known standards (MicroMatter, Deer Harbor, WA) with approximately 5% uncertainty. The mass concentrations were used to perform a principle components analysis that is described in detail in the supplementary information section.

Computer Controlled Scanning Electron Microscopy/Energy Dispersive X-Ray Analysis (CCSEM/EDX). CCSEM/EDX particle analysis was performed at EMSL/PNNL following the campaign. A FEI XL30 digital field emission gun Environmental Scanning Electron Microscope equipped with an EDX microanalysis spectrometer (EDAX, Inc.) was used in this study. Specific details on the CCSEM/EDX analysis of particles collected on the filmed grids are published elsewhere (*2*). The elements detected in particles for this work were C, N, O, Na, Mg, Al, Si, P, S, Cl, K, Ca, Ti, Mn, Fe, Ni, Cr, Zn, and Pb. The atomic percentage data for light elements (C, N, O) are considered semiquantitative (*2*) and therefore were omitted for particle classification purposes. For all other elements, particle composition is reported either as normalized atomic percentage or atomic ratios.

Scanning Transmission X-Ray Microscopy/Near Edge X-Ray Fine Structure Spectroscopy (STXM/NEXAFS). Zinc L-edge NEXAFS spectra and images were acquired using the STXM instrument on beamline 11.0.2 of the Advanced Light Source (Berkeley, CA) in a ~0.5 atm He-filled chamber. The apparatus and experimental method

are described in detail elsewhere (*8-12*). The spatial resolution for these experiments was ~35 nm. Dwell times used to acquire a single energy image were typically 1 ms per pixel. The X-ray energy calibration (±0.1 eV) was afforded by addition of CO_2 gas (~6 Torr) to the STXM chamber through comparison of the position of CO_2 Rydberg transitions at 292.74 and 294.96 eV (*13*).

Standard ZnO, ZnS, $Zn(NO_3)_2 \bullet 6H_2O$, $ZnCl_2$ powders and a 0.05 M solution of $ZnSO_4$ in water were purchased from Sigma-Aldrich (St. Louis, MO). The purity of standard reference materials was ≥ 95%. Thin coatings of the standards were deposited directly onto Si_3N_4 windows by applying gentle contact between the crushed fine powder sample and the Si_3N_4 window and subsequently removing any loose sample. The $ZnSO_4$ solution sample was prepared by placing a small drop on a Si_3N_4 window and then allowing it to evaporate leaving a crystalline residue.

High-Volume Filter Sampling. 24-h integrated samples of $PM_{2.5}$ and PM_{10} were collected at T0 with high volume Tisch samplers (Cleaves, Ohio) equipped with quartz microfiber filters. Filters were stabilized in a controlled temperature and humidity room before and after sampling for gravimetric analysis. Extraction of metals from one half of the filter was carried out with an OI Analytical (College Station, TX) microwave oven using 2 ml of HNO_3, 1 ml of HCl and 2 ml of HF. After digestion the solutions were neutralized with 2% boric acid and gauged. Metals analysis was performed using an ICP-OES (Thermo Jarrel Ash, Waltham, MA). A standard reference material (High Purity, QC-TMFM-A) was used to validate and verify the digestion method accuracy and efficiency, as well as to calculate metal recoveries, percent recovery and traceability coefficients.

2. Single Particle Mixing State and Factor Analysis of Bulk Measurements In the following analysis, we compare single particle mixing states obtained from ATOFMS and CCSEM/EDX data (Figures S1-S4) using the rule based classification scheme detailed in Table S1. As the methodologies behind these techniques are fundamentally different, instrumental characteristics must be considered when comparing the results. In the ATOFMS technique, atomic and molecular ionization efficiencies may differ, and matrix effects may be important for particles of different composition. In turn, CCSEM/EDX provides relative abundance of various elements calculated from EDX spectra as atomic percentages (*2*).

PIXE data compliments the single particle data by supplying quantitative bulk mass concentrations of individual elements ($Z > 11$). Table S2 presents factor loadings obtained using a principal components analysis. Six components of the variation in the elemental concentrations were identified on the basis of the magnitude of eigenvalues (greater than one), and these six factors accounted for 82% of total variance in the entire dataset. The first factor was highly loaded in Al, Si, Ca, Ti, Mg, and Fe. It explained 27% of the total system variance. This factor appears to represent the crustal sources, including air-borne road dust, construction dust, and fugitive dust. The second factor had strong factor loadings for Cl, Na, Zn, and moderately loaded with Pb, Cr, P. It accounted for 22% of the total variance. The fifth factor grouped Cu and K together but with only a slight correlation with Zn, Pb and other metals.

Mixing State of the Me>0, ZnPb>0 Class. To better understand the sources, formation routes and variability of metal rich particles, it is useful to determine the chemical associations (mixing state) in the individual particles. Both the CCSEM/EDX

and ATOFMS can determine the chemical mixing state of single particles. Figure S1 shows stacked bar charts for approximately 4400 (CCSEM/EDX) and 800 (ATOFMS) individual metal containing (Me>0) particles detected shortly after the rain event on March 24th. Stacked bars are plotted for individual particles and the colored area indicates the percent of each metal normalized to sum of all constituents. Potassium was omitted from Figure S1b because it often dominated the ATOFMS signal and hindered our ability to graphically compare mixing states of particles detected with ATOFMS and CCSEM/EDX. Figure S1 clearly shows that Zn, Pb, and Fe are the most abundant metals in the ZnPb>0 class and are internally-mixed. The relative proportions of the Pb max and Zn max particles differ between the two techniques due to the enhanced sensitivity of ATOFMS for Zn and Pb. Additional metals in the ZnPb>0 class include Mg, Al, Ca, Mn, K and Si. Here, Si, Al, and Mg show only minor presence although they are more abundant in the Fe max and "other" unidentified (or organic) classes.

Another way to examine mixing state involves comparing the percentages of particles in a certain class that are mixed with a specific chemical species. In Figure S2, the mixing states of the major classes within the ZnPb > 0 group can be seen for both the ATOFMS (S2a) and CCSEM/EDX (S2b) data sets. Particle classes are indicated on the y-axis and the color scale represents the fraction of the particles in these classes that contain the chemical markers on the x-axis. Both CCSEM/EDX and ATOFMS confirm that Zn and Pb containing particles are strongly mixed with Na, K, and Cl. Within the Zn max class, both CCSEM/EDX and ATOFMS data show a strong association with sulfate (detected as S in the EDX spectra). The ATOFMS data indicate that the secondary nitrogen markers $^{46}NO_2^-$ and $^{62}NO_3^-$ are strongly coupled with all particles containing Zn

and Pb although the amount of NO_3 is a strong function of the time of day due to the nitrate/chloride heterogeneous chemistry described in the main manuscript. Phosphorous markers ($^{79}PO_3^-$, $^{95}PO_4$), represented in Figure S2a as PO, are found to be mainly associated with the ZnPb > 0 set and weakly associated with Me>0, Pb & Zn = 0 particles. The CCSEM/EDX measurements reveal that P is mostly present in the ZnPb>0 class as well, but in fewer particles. This result suggests that P is a trace element in ZnPb>0 particles.

As seen in Fig S2a, ~50% of the ZnPb>0 particles were also mixed with carbon. Compared to Me>0, Pb & Zn = 0 classes, the ZnPb>0 classes contain a higher fraction of particles with a $^{36}C_3^+$ peak. This marker is an important identifier for elemental carbon (EC), and indeed EC was most strongly mixed within the ZnPb>0, Zn max type. This was further corroborated by the STXM/NEXAFS identification of soot in Zn-containing particles.

A cluster accounting for 6.3% of the total Pb containing particles contained Cu, EC, oxalate, Zn, and Pb. Here, this is reflected in the fact that Zn max particles also contain a higher proportion of Cu and oxalate ion ($C_2O_4^{-2}$). Approximately 65% of the Zn max particles contain the oxalate marker (Fig S2a). Although the exact reason for this is not known, it is common knowledge that oxalate binds strongly to metal ions within fog water (*14*). The formation of metal-oxalate complexes from the constituent ions has an equilibrium constant $K_{eq} > 10^6\ M^{-1}$ and increases with the metal oxidation state. If the metals are present along with hot water vapor in industrial emissions, oxalate complexes may form in the aqueous particles.

Most of the ZnPb>0 particle classes are strongly associated with traces of alkali metals (Li, Na and K). Most of the particle classes analyzed with the ATOFMS contain K and Li. The CCSEM/EDX data in Fig S2b shows that K is primarily associated with the ZnPb>0 classes, with the exception of the Pb=0, K max type. Given that the CCSEM/EDX primarily detects K in the ZnPb>0 particle type while the ATOFMS detects K in most particle classes suggests the concentration of K in the ZnPb>0 particle classes is higher than in the other particle classes. These mixing state relationships are confirmed by the PIXE factor analysis detailed above. Specifically, Zn and Cl are correlated with Na, Pb, and P all of which were found to be internally mixed by the single particle techniques.

Mixing State of the Pb & Zn=0, Me>0 Class. Many of the particles that were detected after the heavy rain event did not contain Zn or Pb, but were frequently associated with the early morning industrial plumes. Figure S3 graphically presents approximately 1500 (CCSEM/EDX) and 360 (ATOFMS) particles from the Me>0, ZnPb = 0 class. The most dominant subclass of the Me>0, Pb & Zn = 0 class was identified as Na max in both CCSEM/EDX and ATOFMS data. As seen in Fig. S2a, this particle class has a significant contribution from Cl, suggesting NaCl as the primary species. This is further evidenced by the fact that many of the particles containing Na and Cl had a cubic shape. From the CCSEM/EDX data, an average composition of $Na_{1.00}Cl_{0.74}S_{0.24}Si_{0.06}OE_{<0.05}$ (*OE*-other elements) was determined, suggestive of mixed sodium chloride and sodium sulfate particles. Sodium nitrate may be present: the ATOFMS data showed that ~70% of the Na max particles contain nitrate species. The

occasional presence of Mg at low concentrations indicates that a sea salt source is unlikely. However, waste incineration is known to produce NaCl particles (*15*).

As noted above, the primary difference between the CCSEM/EDX and ATOFMS data is the higher abundance of K max particles in the ATOFMS data set. Additionally, fewer Fe max particles were identified with ATOFMS than with the CCSEM/EDX. Li is more abundant in the Na max class while K max are deficient Li. It may be that there is simply less Li in the K max particles, or alternatively, that a matrix effect in the K max particles suppresses the formation of Li^+ ions. Further differences in the K max and Na max particle classes are observed in Figure S3. For example, Na max is more abundant in $^{35}Cl^-$, $^{79}PO_3^-$, and Si markers while K max has more $^{12}C^+$. This indicates that the Na max particle type is more strongly associated with common inorganic markers (Cl, Si, and P), whereas the K max type is more commonly associated with carbonaceous and secondary nitrate and sulfate markers.

Me=0 Particles Fig S2 shows that the Me=0 class was primarily composed of organic and elemental carbon species. These organics include a strong signature from the elemental carbon marker at m/z=36 as well as aromatic markers at m/z = 50, 51 and 77. These aromatic markers were found to be in 13-15% of the Pb and Zn rich classes. Over 75% of the Me=0 class contained these aromatic markers. It is also important to note that this aromatic containing particles within the Me=0 class had detectable levels of Cl, with 8% of the particles having a detectable signal for Cl at m/z=-35. This may indicate the presence of chlorinated organic compounds.

Chloride and Nitrate in Zn and Pb Rich Particles. Both ATOFMS and CCSEM/EDX techniques show that Pb-max particles are mixed with Cl. Ternary plots showing the distribution of Pb, S, N, and Cl for Pb Max particles are shown in Figure S4. In Figs. S4 a and c, ATOFMS shows the distribution of S, N and Cl, where S represents the sum of $^{32}S^-$, $^{64}SO_2^-$ $^{80}SO_3^-$ and $^{97}HSO_4^-$, and N represents the sum of $^{46}NO_2^-$ and $^{62}NO_3^-$. For the Pb max particles, N and Cl dominate the ATOFMS peak areas. CCSEM/EDX shows that Cl is present in both Pb max and Zn max, but Cl is much more prevalent in the Pb max particle type. This could be because of contributions from the ZnO class and/or reaction with acidic gases.

Table S1. Rules used to define particle classes over ATOFMS and CCSEM/EDX data sets

Particle Set	ATOFMS Rules	SEM/EDX Rules
Total	Time = [24-Mar-2006 5:15:00 24-Mar-2006 5:30:00]	Time = [24-Mar-2006 5:15:00 24-Mar-2006 5:30:00]
Zn>0	Area{64}>50 and Area{66}>50 and Area{68} > 50	N/A
Pb>0	mean(area{205 209})/mean(area{210 230}) >5	N/A
K>0	mean(area{39})/mean(area{36 38}) >2.5	N/A
Na>0	Area{23} > 50	N/A
Mg>0	Area{24}>3xArea{25} and Area{24}>3xArea{26}	N/A
Cu>0	Area{63+65}>3xArea{60+61+62}	N/A
Fe>0	Area{54}>100 and Area{56}>1000	N/A
Me>0	(Zn∩Pb∩K∩Na∩Mg∩Fe) >0	(Pb∩Fe ∩Mg∩Zn∩Si∩Al∩Mn∩K) > 0
Me=0	Total – Me>0	N/A
ZnPb>0, Pb max	(Me>0 ∪ Pb>0) ∪ Pb>Fe,Mg,Zn	(Me>0 ∪ Pb>0) ∪ Pb>Fe,Mg,Zn,Si,Al,Mn,K
ZnPb>0, Zn max	(Me>0 ∪ Pb>0) ∪ Zn>Pb, Fe, Mg	(Me>0 ∪ Pb>0) ∪ Zn>Fe,Mg,Si,Al,Mn,K
ZnPb>0, Fe max	(Me>0 ∪ Pb>0) ∪ Fe>Pb,Mg,Zn	(Me>0 ∪ Pb>0) ∪ Fe>Mg,Zn,Si,Al,Mn,K
ZnPb>0, Mg max	(Me>0 ∪ Pb>0) ∪ Mg>Pb,Fe,Mg	(Me>0 ∪ Pb>0) ∪ Mg>Fe,Zn,Si,Al,Mn,K
Me>0, Pb=0	Me>0∪Pb=0	Me>0 ∪ Pb=0
Me>0, ZnPb=0	Me>0 ∪ Pb=0 ∪ Zn=0	Me>0 ∪ Pb=0 ∪ Zn=0
Me>0, ZnPb=0, Na max	(Me>0, Pb & Zn=0) ∪ Na>K,Fe,Mg,Al	(Me>0, Pb & Zn=0) ∪ Na>K,Fe,Mg,Si,Al,Mn
Me>0, ZnPb=0, K max	(Me>0, Pb & Zn=0) ∪ K> Na,Fe,Mg,Al	(Me>0,Pb & Zn=0) ∪ K>Na,Fe,Mg,Si,Al,Mn
Me>0, ZnPb=0, Fe max	(Me>0, Pb & Zn=0) ∪ Fe> K,Na,Mg,Al	(Me>0, Pb & Zn=0) ∪ Fe>K,Na,Mg,Si,Al,Mn
Me>0, ZnPb=0, Mg max	(Me>0, Pb & Zn=0)∪Mg> K,Na,Fe,Al	(Me>0, Pb & Zn=0) ∪ Mg> K,Na,Fe,Si,Al,Mn
Me>0, ZnPb=0, Al max	(Me>0, Pb & Zn=0) ∪ Al> K,Na,Mg,Fe	(Me>0, Pb & Zn=0) ∪ Al> K,Na,Fe,Mg,Si,Mn

Table S2. Summary of the factor analysis performed on the PIXE elemental mass concentrations.

	Factor1	Factor2	Factor3	Factor4	Factor5	Factor6	Community
Al	**0.962**	0.088	0.024	0.123	-0.03	0.034	0.883
Si	**0.958**	0.141	0.061	0.123	0.014	0.012	0.857
Ca	**0.92**	0.137	0.051	-0.088	0.223	0.101	0.95
Ti	**0.878**	0.08	-0.044	-0.183	0.268	0.067	0.958
Mg	**0.87**	0.143	0.127	0.186	-0.157	0.063	0.675
Fe	**0.801**	0.301	0.105	-0.176	0.375	-0.021	0.835
Mn	0.468	0.458	0.293	-0.187	0.317	-0.17	0.885
Cl	0.097	**0.906**	-0.115	0.002	0.127	0.161	0.935
Na	0.342	**0.827**	-0.059	0.228	-0.154	0.061	0.889
Zn	0.111	**0.801**	-0.075	-0.021	0.297	0.158	0.822
Pb	0.097	**0.754**	0.253	-0.125	-0.048	0.031	0.697
Cr	0.256	**0.719**	0.059	0.324	0.01	-0.085	0.679
P	-0.014	**0.687**	0.302	0.24	0.155	-0.174	0.916
Ni	0.125	0.253	**0.853**	0.146	-0.044	0.045	0.904
V	0.07	-0.153	**0.847**	0.264	0.072	0.029	0.833
Hg	-0.026	0.111	0.223	**0.84**	0.061	-0.016	0.722
S	0.006	0.256	**0.533**	**0.696**	-0.019	0.008	0.774
Cu	0.071	0.268	-0.037	-0.134	**0.75**	0.251	0.66
K	0.286	-0.063	0.071	0.378	**0.723**	0.041	0.772
Co	0.125	0.093	0.066	-0.007	0.205	**0.913**	0.758
EV	5.416	4.326	2.093	1.845	1.681	1.044	
% of Variance	27.08	21.631	10.466	9.223	8.405	5.22	
Cumulative %	27.08	48.711	59.177	68.399	76.805	82.025	

Extraction Method: Principal Component Analysis.

Rotation Method: Varimax with Kaiser Normalization.

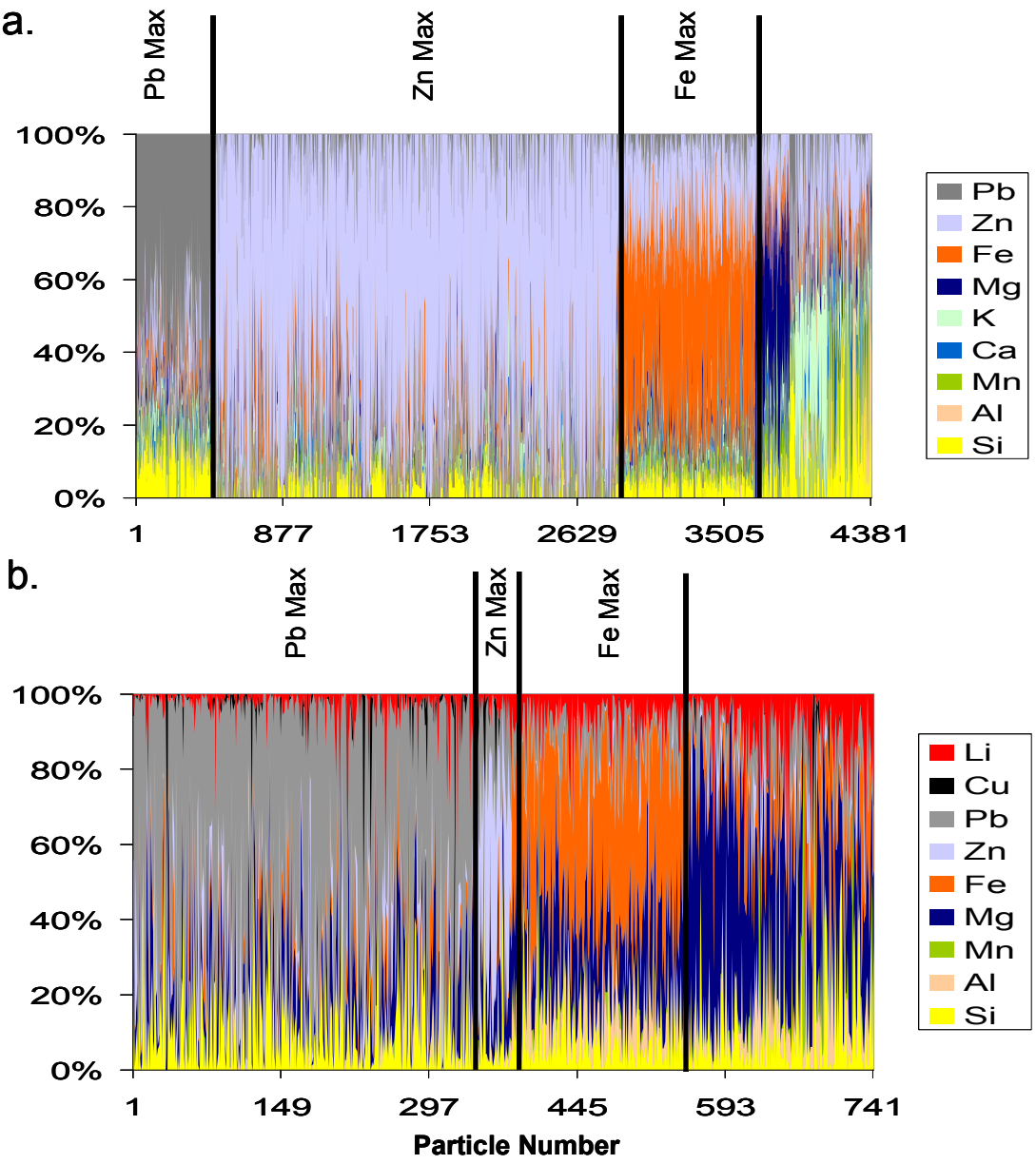

Figure S1. Chemical associations (mixing state) for single particles containing Zn and Pb sampled on Mar, 24 5:15-5:30 UTC derived from the CCSEM/EDX (Top) and the ATOFMS (Bottom) data sets.

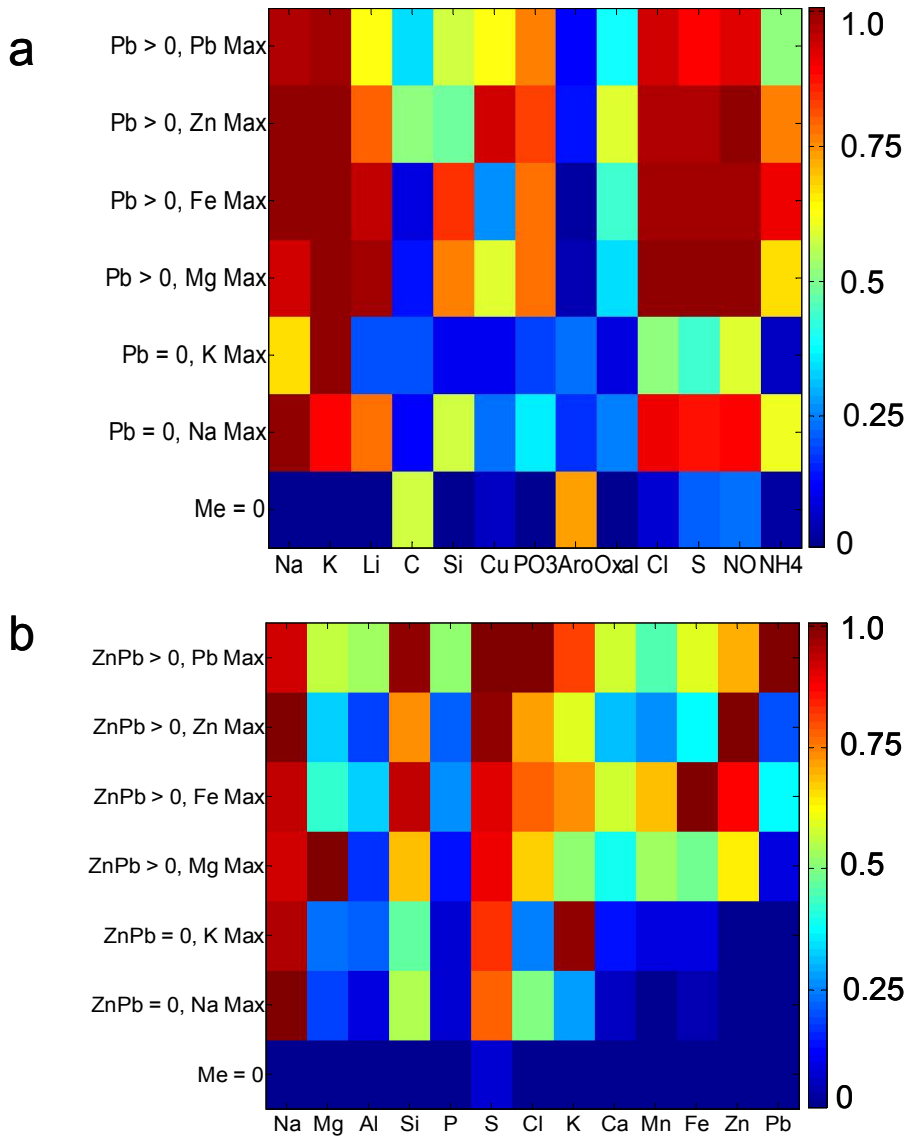

Figure S2. Mixing state of metal containing particles analyzed on Mar 24 derived from the ATOFMS (panel (a)) and CCESM/EDX (panel (b)) data sets. The color axis gives the fraction of particles on the y axis that contain the markers shown on the x axis. All classes and markers are defined in Table S2.

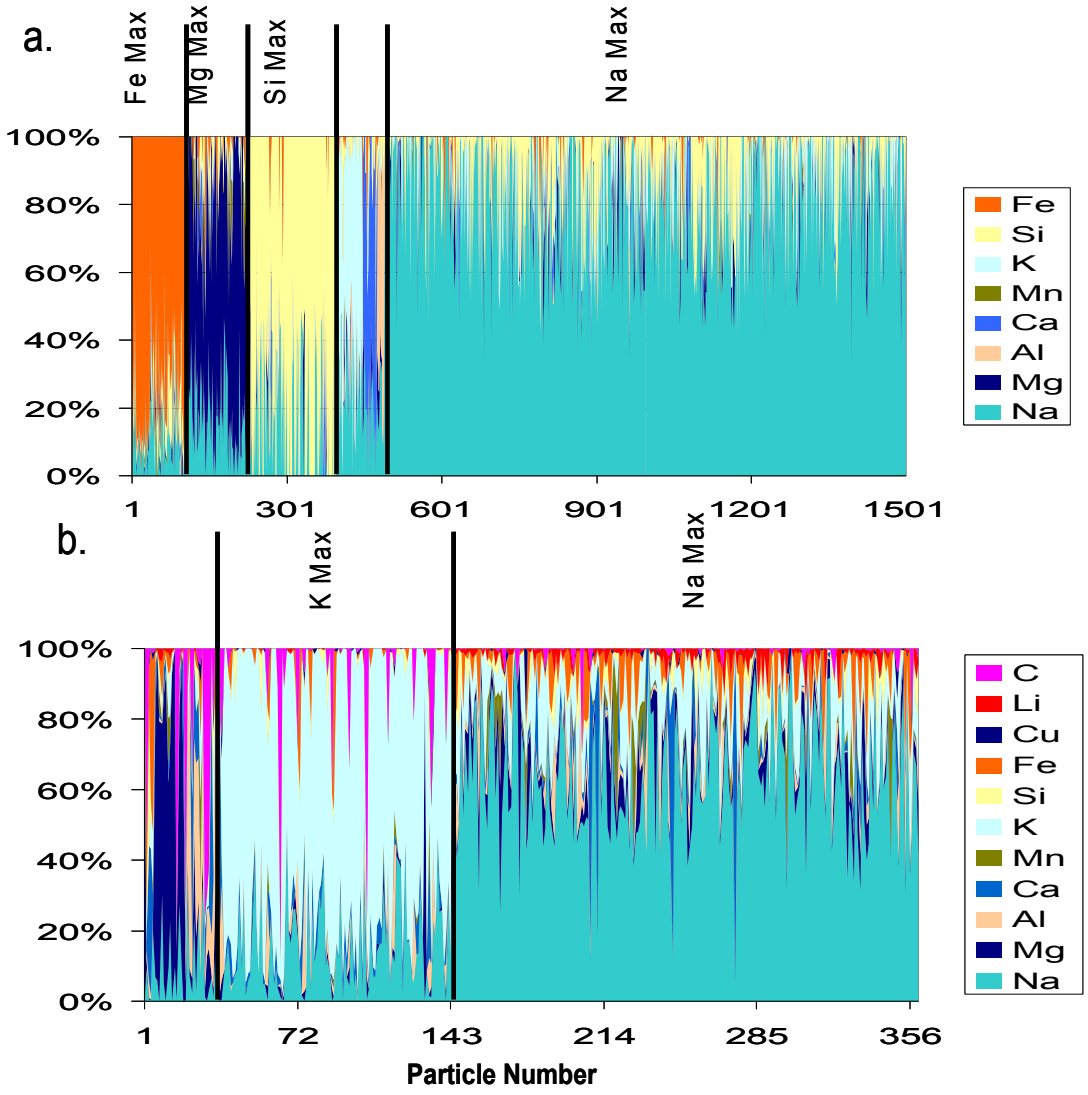

Figure S3. Chemical associations (mixing state) for single particles that do not contain Zn and Pb sampled on Mar, 24 5:15-5:30 UTC derived from the CCSEM/EDX (panel a) and the ATOFMS (panel b) data sets.

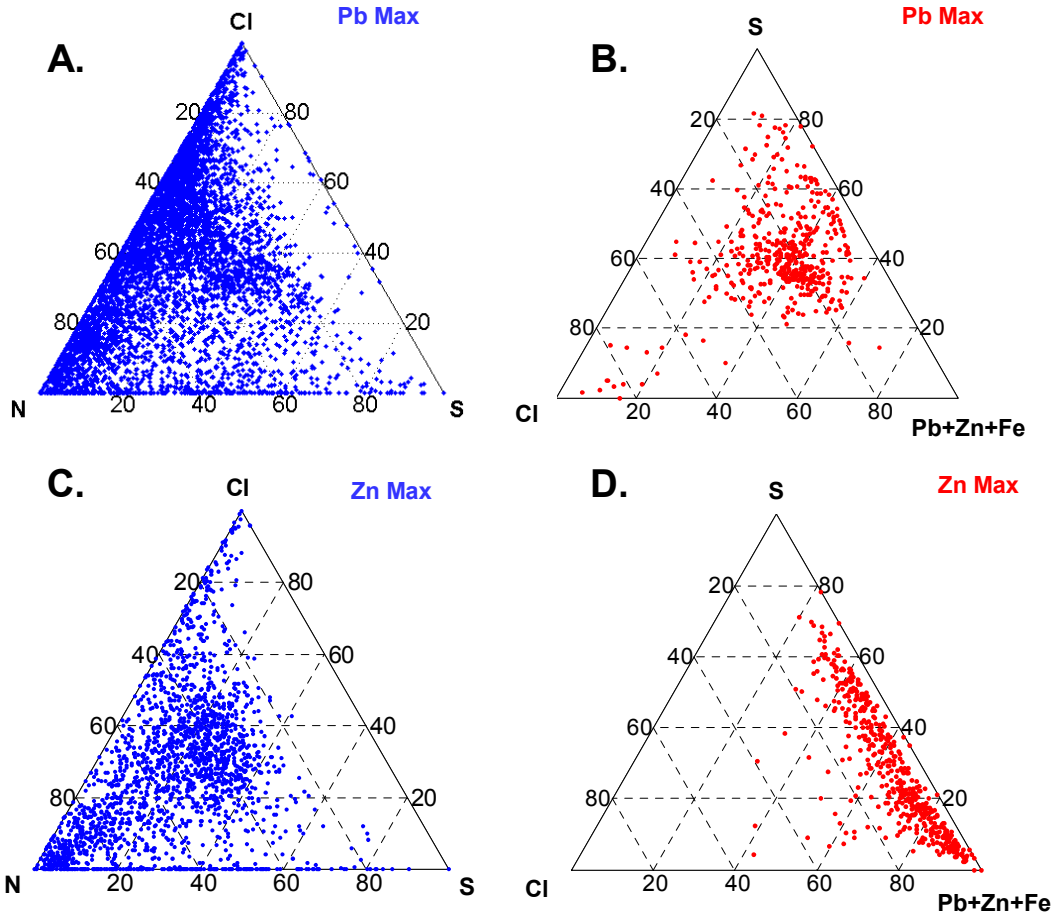

Figure S4. Ternary plots illustrating the chemical composition of secondary/primary species N, Cl, and S. A) N-S-Cl ternary diagram for submicron Pb max particles B) **(**FeZnPb)-S-Cl ternary diagram showing CCSEM/EDX-measured compositions of "Me>0, Pb >0, Pb max**"** individual particles (yellow dots). Red dots correspond to nominal values of various PbCl2/PbSO4 mixtures C) N-S-Cl ternary diagram for submicron Zn max particles D) **(**FeZnPb)-S-C ternary diagram showing CCSEM/EDX-measured compositions of "Me>0, Pb >0, Zn max" individual particles

References

(1) Cahill, T. A.; Wayakabashi, P. Compositional analysis of size segregated aerosol samples *ACS Adv. Chem. Ser.* **1993**, *232*, 211-228.
(2) Laskin, A.; Cowin, J. P.; Iedema, M. J. Analysis of individual environmental particles using modern methods of electron microscopy and X-ray microanalysis *J Electron Spectrosc* **2006**, *150*, 260-274.
(3) Laskin, A.; Iedema, M. J.; Cowin, J. P. Time-resolved aerosol collector for CCSEM/EDX single-particle analysis *Aerosol Sci. Technol.* **2003**, *37*, 246-260.
(4) Gard, E.; Mayer, J. E.; Morrical, B. D.; Dienes, T.; Fergenson, D. P.; Prather, K. A. Real-time analysis of individual atmospheric aerosol particles: Design and performance of a portable ATOFMS *Anal. Chem.* **1997**, *69*, 4083-4091.
(5) Moffet, R. C.; Prather, K. A. Extending ATOFMS measurements to include refractive index and density *Anal. Chem.* **2005**, *77*, 6535-6541.
(6) Shutthanandan, V.; Thevuthasan, S.; Disselkamp, R.; Stroud, A.; Cavanagh, A.; Adams, E. M.; Baer, D. R.; Barrie, L. A.; Cliff, S. S.; Jimenez-Cruz, M.; Cahill, T. A. Development of PIXE, PESA and transmission ion microscopy capability to measure aerosols by size and time *Nucl Instrum Meth B* **2002**, *189*, 284-288.
(7) Maxwell, J. A.; Campbell, J. L.; Teesdale, W. J. The Guelph Pixe Software Package *Nucl Instrum Meth B* **1989**, *43*, 218-230.
(8) Drake, I. J.; Liu, T. C. N.; Gilles, M.; Tyliszczak, T.; Kilcoyne, A. L. D.; Shuh, D. K.; Mathies, R. A.; Bell, A. T. An in situ cell for characterization of solids by soft x-ray absorption *Rev Sci Instrum* **2004**, *75*, 3242-3247.
(9) Hopkins, R. J.; Tivanski, A. V.; Gilles, M. K. Chemical Bonding and Structure of Black Carbon Reference Materials and Individual Carbonaceous Atmospheric Aerosols *J. Aerosol Sci.* **2007**, *38*, 573-591.
(10) Maria, S. F.; Russell, L. M.; Gilles, M. K.; Myneni, S. C. B. Organic aerosol growth mechanisms and their climate-forcing implications *Science* **2004**, *306*, 1921-1924.
(11) Michelsen, H. A.; Tivanski, A. V.; Gilles, M. K.; van Poppel, L. H.; Dansson, M. A.; Buseck, P. R. Particle formation from pulsed laser irradiation of soot aggregates studied with a scanning mobility particle sizer, a transmission electron microscope, and a scanning transmission X-ray microscope *Appl. Opt.* **2007**, *46*, 959-977.
(12) Tivanski, A. V.; Hopkins, R. J.; Tyliszcazak, T.; Gilles, M. K. Oxygenated Interface on Biomass Burn Tar Balls Determined by Single Particle Scanning Transmission X-ray Microscopy *J. Phys. Chem. A* **2007**, *111*, 5448-5458.
(13) Ma, Y.; Chen, C. T.; Meigs, G.; Randall, K.; Sette, F. High-Resolution K-Shell Photoabsorption Measurements of Simple Molecules *Physical Review A* **1991**, *44*, 1848-1858.
(14) Sedlak, D. L.; Hoigne, J. The Role of Copper and Oxalate in the Redox Cycling of Iron in Atmospheric Waters *Atmos. Environ.* **1993**, *27*, 2173-2185.
(15) Wilewska-Bien, M.; Lundberg, M.; Steenari, B. M.; Theliander, H. Treatment process for MSW combustion fly ash laboratory and pilot plant experiments *Waste Managment* **2007**, *27*, 1213-1224.